RSC Advances

ROYAL SOCIETY OF CHEMISTRY

www.rsc.org/advances

Highly selective arylhydrazone based "ON–OFF" fluorescent chemosensor for Zn^{2+} ion, inhibitors for KB cell, 4LRH cancer protein and DFT studies

Annamalai Subhasri and Chinnadurai Anbuselvan*

Department of Chemistry, Annamalai University, Annamalainagar − 608 002, India

Corresponding author email: cas_amu@yahoo.co.in

*Corresponding author: Address

Dr. C. Anbuselvan

Assistant professor,

Department of Chemistry

Annamalai University

Annamalainagar 608 002

E-mail: *cas_amu@yahoo.co.in*

Synthesis of hydrazone-based chemosensor assemblies for zinc is detailed in this report using established and simple synthetic pathways. The coordination properties and photo physical response of new, easy-to-prepare and highly selective 2-(2-(4-fluoro-2-nitrophenyl)hydrazono)-5,5-dimethylcyclohexane-1,3-dione **(1)**, (*E*)-5,5-dimethyl-2-(2-(4-(phenyldiazenyl)phenyl)hydrazono)cyclohexane-1,3-dione **(2)** have been examined. The sensors were characterized by UV-Vis, FT-IR, ^{1}H NMR, ^{13}C NMR, scanning electron microscopy (SEM) and fluorescence spectroscopy. New sensors exhibited higher selectivity for Zn^{2+} over other metal ions in aqueous ethanol medium. The experimental results show chemosensor is highly selective and sensitive towards Zn^{2+} in the presence of competing ions, even in the lower concentration with a detection limit of 3.5 µM **(1)** and 4.0 µM **(2)**. A collective experimental and theoretical studies were carried out on the molecular structure using density functional methods (B3LYP) invoking 6-31G basis set. From the theoretical studies energy of the highest occupied molecular (HOMO) orbital and lowest unoccupied (LUMO) molecular orbital have been predicted. From the cytotoxic study, the ability of these compounds **(1)** and **(2)** to inhibit the growth of KB cell lines was examined. Chelating functionality of compound **(1)** and **(2)** were evaluated for their inhibitory properties against various cancer proteins like 4LRH, 4EKD, 4GIW and 4L9K.

Introduction

A fluorescent chemosensor is a molecular system in which the physiochemical properties change upon interaction with a chemical species, so that an alteration in fluorescence is produced. The construction of a fluorescent chemosensor generally involves two integrated components. One is a signaling fluorophore and another one is a guest receptor that possesses a detection capability. Both are connected by a spacer to form a so-called fluorophore–spacer–receptor scaffold. The guarantee of fluorescent detection is superior to other analytical techniques because of its highly promising prosperities like sensitivity, simplicity of usage, and low expenditure.[1–6]

Zinc ion (Zn^{2+}) is paying attention to a vast deal of an awareness ascribing to the biological significance. Zinc is the second most abundant transition metal ion in the human body after iron (2.3 g Zn for a normal person).[7] Zn^{2+} is now recognized as one of the most important cations in catalytic centers and structural cofactors of many Zn^{2+}containing enzymes and DNA-binding proteins (e.g., transcriptions factors) and it is a vital constituent of various protein scaffolds (e.g., carbonic anhydrase and zinc finger protein).[8] Zinc has been well-known to act as a structural component of proteins or in the catalytic site of enzymes[9,10] and plays very important role in gene transcription and metallo enzyme function.[11] In addition, the neurobiology of Zn(II) has become a subject of increasing awareness [12, 13] and a key element involved in a plethora of biological processes, such as cellular metabolism, neurotransmission, apoptosis and is also drawn in the pathophysiological consequences manifested in several diseases such as Alzheimer's

disease, epilepsy, ischemic stroke, and infantile diarrhea, brain function and pathology, gene transcription, immune function, and mammalian reproduction,[14–16]

Zn^{2+} is essential for wound healing and supports the healthy growth and development of the body during adolescence, childhood and pregnancy. Even though most Zn^{2+} is strongly bound to enzymes and proteins, free zinc pools survive in some tissues such as the brain, intestine, pancreas, and retina. Because Zn^{2+} is spectroscopically silent due to its d^{10} electronic configuration, many fluorescent chemosensors for the detection of Zn^{2+} have been studied intensively.[17,18] Several reviews have focused on various aspects of zinc fluorescent chemosensors.[19–26] An enhancement of fluorescent molecular sensors for the detection of these metal cations is of great awareness in environmental and biological chemistry.

Hydrazones are significant precursors for the production of heterocycles, pharmaceuticals, agrochemicals, polymers, dyestuffs and photography. Aryl hydrazones are important classes of compounds which have long fascinated attention, owing to their significant biological and pharmacological applications such as antibacterial, antiviral, antineoplastic, and antimalarial activities.[27] The arylhydrazone exhibits very high fluorescence behavior. Fluorescent organic compounds have been widely used as fluorescent markers in chemistry, biology and medicine for molecular visualization and in particular for visualization of enzyme activity[28, 29]. The design and synthesis of a sensitive and selective fluorescent sensor is an essential goal for both organic and analytical chemists. Therefore, research on metal-ion-selective fluorescent chemosensors have attracted a great attention from chemical scientists, and great achievements have been obtained.[30–33]

In this article, we describe the synthesis, characterization and selective recognition behavior of aryl hydrazone derivatives as a highly efficient chemosensors for Zn^{2+}. Our

sensors show extremely high selectivity compared to the other recently developed Zn^{2+} sensors which is attributed to the very high association constants for the binding of Zn^{2+}.

Materials and Method

All chemicals and solvents were of analytical grade as obtained from commercial suppliers and were used directly without further purification. Thin layer chromatography (TLC) was performed on TLC aluminum sheets covered with silica gel (0.2 mm). NMR spectra: measured in $CDCl_3$ at 400 MHz for ^1H and 125 MHz for ^{13}C. The δ values are given in ppm relative to TMS as internal standard, and the chemical shift of the TMS peak was set to 0 ppm for ^1H and ^{13}C NMR spectra (Bruker instrument). IR spectra were recorded on an Avatar Nicholet FT-IR spectrophotometer (range 4000–400 cm^{-1}) in KBr pellets (λ_{max} in cm^{-1}). UV–vis spectra were recorded on a SHIMADZU UV-1650 PC digital spectrophotometer by dissolving the sample in spectral grade ethanol using a 1 cm path length quartz cell. A Perkin Elmer LS 55 fluorescence spectrometer was used to record the fluorescence (FL) spectra at room temperature. The choice of excitation wavelengths was based on the absorbance spectral characteristics.

Compounds **(1)** and **(2)** were prepared by the general procedure (Scheme 1) in which anilines (0.5 mmol) were dissolved separately in 1 N HCl (25 cm^3) at 0–5 °C temperature and in each case cooled aqueous solution (10 cm^3) of $NaNO_2$ (0.40 g) was added drop wise with stirring followed by the addition of dimedone (0.70 g, 0.5 mmol) and sodium acetate (5.0 g) dissolved in water (30 cm^3). The obtained mixture was further stirred for 4 h at room temperature (25 °C). Solid thus obtained were filtered and washed several times with water, followed by ethanol and then dried in a vacuum. The crude products were recrystallized in

ethanol. Compounds **(1)** and **(2)** were purified by column chromatography by using benzene as an eluent. Yield and melting points of the derived compounds are mentioned below.

Estimation of Metal salts.

A stock solution of compound 1 (3.0×10^{-3}M) and 2 (1.0×10^{-3} M) were prepared in CH_3CH_2OH/H_2O (4:1, v/ v). Solutions of 2.0×10^{-4} M salts of the respective cations were prepared in distilled water. All experiments were carried out in CH_3CH_2OH/H_2O solution (CH_3CH_2OH/H_2O = 4:1, v/v, 10 μM HEPES buffer, pH = 7.0). In titration experiments, each time at 4×10^{-5} M solution of 1 and 2 were filled with a quartz optical cell of 1 cm optical path length, and the ion stock solutions were added into the quartz optical cell gradually by using a micropipette. Spectral data were recorded for 1 min after the addition of the ions. In selective experiments, the test samples were prepared by placing appropriate amounts of the anions/ cations stock into 2 mL of solution of 1 (3.0×10^{-3} M) and 2(1.0×10^{-3} M).

Molecular Docking

Molecular docking was performed by *Glide* module implemented in *Maestro* version 9.3.5 of the Schrödinger software suite, 2011. The ligands were prepared by *Ligprep* application in which the conformers were generated using a rapid torsion angle search approach followed by minimization of each generated structure using the OPLS-2005 (Optimized Potential for Liquid Simulations) force field. The 3D coordinates of crystallographic structure of the (PDB ID: 4LRH, 4EKD, 4GIW and 4L9K) were downloaded from Brookheaven protein Data Bank (www.rscb.com). The protein complex was pre-processed and prepared by *a Protein Preparation Wizard* in Maestro of Schrödinger. The minimization of the complex was continued using OPLS-2005 force field until the root mean square deviation (RMSD) reached the value of 0.3 Å. The molecular docking studies of the ligands

and the protein were performed by GLIDE. Glide provides three different levels of docking precision (HTVS), high throughput virtual screening (SP), standard precision, and (XP), extra precision. We carried out calculations in XP mode. The best fit molecules with the protein were ranked based on the G score. We have used the following software for molecular docking. Software version 1. Maestro version 9.3.5. Schrödinger, LLC, New York, 2011. 2. Schrödinger Suite 2011, Protein Preparation Wizard; Epik version 2.2; Impact version 5.7, Schrödinger, LLC, New York, 2011, 3. Glide, version 5.7, Schrödinger, LLC, New York, 2011, 4. LigPrep, version 2.5, Schrödinger, LLC, New York, 2011.

Anticancer activity

Cell culture

The KB cancer cell line was obtained from NCCS (National Centre for Cell Science, Pune). The cells were cultured in Dulbecco's modified Eagle's medium (DMEM, Sigma Aldrich) which was supplemented with 10% fetal bovine serum. The cells were grown at 37 °C under a humidified 5% CO_2 atmosphere.

Cell viability assay

The cytotoxicity of compounds **(A)** and **(B)** were tested against KB cell lines using the 3-(4,5-dimethylthiazole-2-yl)-2,5-diphenyl tetrazolium bromide (MTT) assay.[34] The cells were seeded into a 96-well plate at a density of 1.5×104 cells per well and incubated in medium containing compounds **(A)** and **(B)** at concentrations ranging from 1.5 to 500 μM for 48 h. Triplicate wells were maintained for each treatment. To each well, 100 μL of MTT was added and the plates were incubated at 37 °C for 4 h to allow MTT to form formazan crystals by reacting with metabolically active cells. The medium with MTT was removed

from the wells. Intracellular formazan crystals were dissolved by adding 100 μL of DMSO to each well and the plates were shaken for 10 min. The absorbance was observed at 570 nm and 630 nm is using an enzyme linked immunosorbent assay (ELISA) reader and the cell images were examined using a fluorescence microscope. The percentage of survival was calculated using the formula:

% survival = [live cell number (test)/live cell number (control)] × 100.

Computational details

The entire calculations were performed at ab initio DFT levels using Gaussian 03W[35] program package, invoking gradient geometry optimization.[36] Initial geometry generated from standard geometrical parameters was minimized without any constraint in the potential energy surface at ab initio adopting the standard 6-31G basis set.

2-(2-(4-fluoro-2-nitrophenyl)hydrazono)-5,5-dimethylcyclohexane-1,3-dione (1)

Yellow solid, yield: 91 %, m. p. 192 °C; IR (KBr, cm^{-1}) 3420, 2958, 2927, 2872, 1684, 1645, 1590 **(Fig. S1)**; ^{1}H NMR (400 MHz, CDCl$_3$) (δ): 2.64 and 2.61(s, CH$_2$), 1.08(s, CH$_3$) 7.19–8.33 (aromatic protons), 15.90 (s, NH) **(Fig. S3)**; ^{13}C NMR (125 MHz, CDCl$_3$) (δ) 28.6, 30.6, 52.9, 53.0, 112.4, 112.6, 120.7, 120.8, 123.8, 124.1, 132.7, 134.8 **(Fig. S4).**

(E)-5,5-dimethyl-2-(2-(4-(phenyldiazenyl)phenyl)hydrazono)cyclohexane-1,3-dione (2)

Orange solid, yield: 82 %, m. p. 195 °C; IR (KBr, cm^{-1}) 3424, 2955, 2924, 2853, 1679, 1639, 1615 **(Fig. S2)**; ^{1}H NMR (400 MHz, CDCl$_3$) (δ): 1.16 (s, CH$_3$), 2.65 (s,CH$_2$) 7.27–8.02 (aromatic protons), 15.43 (s, NH) **(Fig. S5)**; ^{13}C NMR (125 MHz, CDCl$_3$) (δ) 28.6, 30.8, 52.7, 108.5, 117.9, 120.0, 122.9, 124.6, 129.2, 156.8, 193.4, 197.5 **(Fig. S6)**.

Results and discussion

The compounds 2-(2-(-4-fluoro-2-nitrophenyl)hydrazono)-5,5-dimethylcyclo hexane-1,3-dione **(1)** and (*E*)-5,5-dimethyl-2-(2-(4-(phenyldiazenyl)phenyl)hydrazono) cyclohexane-1,3-dione **(2)** have been synthesized and their IR spectra of **(1)** and **(2)** show ν(NH) vibration at 3420–3424 cm^{-1}, while ν(C=O), ν(C=O......H) and ν(C=N) are observed at 1718–1711, 1664–1671 and 1539–1592 cm^{-1}, respectively (**Fig. S1** and **S2**). These bands can be related to the hydrogen bonded hydrazone fragment. This conclusion is additionally supported by the ^{1}H and ^{13}C NMR data, e.g. the ^{1}H NMR spectra of **(1)** and **(2)** show signals at 15.90 –15.43 ppm which can be assigned to the proton of the NH moiety adjacent to aryl unit because of strong intramolecular hydrogen bonding. In compound **(1)** and **(2)** the aromatic proton signals appear in the downfield region of 6.95–7.96 ppm with the expected splitting patterns (**Fig. S3** and **S5**). Carbonyl sp^2 carbon atoms appear as separate signals in the low field region of about 186 and 188 ppm for C-A and C-B, respectively. Strong intramolecular N–H……O–C hydrogen bonding deshields C-A with respect to C-B to the extent of ca. 2 ppm (**Fig. S4** and **S6**).

Scanning electron microscopy (SEM) was used to analyze the surface morphology self-assembled microstructure of the resulting compounds. The morphologies of the compounds (**1**) and (**2**) were observed to be different depending on the ligand group at the para-position, i.e., Fluorine and phenyldiazenyl. Platinum was coated on the surfaces of samples and images of (**1**) at 10 and 5 μm are shown in Fig. 1a and c, respectively. The ligand (**1**) shows a micro rod like structure and the particle size of Fluorine substituted hydrazone is around 10–15 μm diameter (Fig. 1c) and surface of the micro rod fully rough and made up of huge amounts of particles. We observed a considerable change in the

morphology of ligand when Zinc ion was added to **(1)** (formation complex with Zn^{2+}). The surface morphology of the complex of **(1)** with the Zn^{2+} ion shows the agglomeration of the surface structure covered with a large amount of spherical particles (Fig. 1b and d). The ligand **(2)** displayed a grass like structure (Fig. 2a and c). The complex of **(2)** with the Zn^{2+} ion shows self-assembled flower like structure (Fig. 2b and d).

Solvatochromism

The solvatochromic studies of compounds (1) and (2) were carried out in 15 solvents of varying polarity and the absorption spectra shown in Fig. S7A and S7B. This band is associated with charge transfer from N-H group to the carbonyl oxygen (C=O) due to intramolecular hydrogen bonding between them. This intramolecular hydrogen bond is responsible for the stabilization of the charge transfer band. In particular for hydrazone derivatives charge transfer between a donor part, N–H (D) and an acceptor part, 1,3-dione (1), has been considered. Both donor and acceptor appear to be localized in the quasi aromatic rings containing the intramolecular hydrogen bonds. So, this hydrogen-bonded quasi-aromatic ring contributes stabilization of the charge transfer band. Generally, a shift of the absorption maximum in various solvent exhibits mainly depends on the strength of the hydrogen bond between the substituent and solvent molecules. In the present case, the important feature observed is that the absorption band undergoes a hypsochromic shift with increasing solvent polarity. Further, this band shift is very small while changing the polarity of the solvents. The observed difference in the absorption band shift measured in a nonpolar solvent (hexane) and a dipolar aprotic solvent (DMSO) is only 14 nm and 16 nm respectively. This is expected since the specific interactions of compound **(1)** and **(2)** with these solvents are quite diminished by the strong intramolecular hydrogen bond between the

–C=O and N–H groups. The dipolar aprotic solvents do not contribute much in the case of band shift in the ground state of the compounds **(1)** and **(2)** indicating that even hydrogen – bond donor solvents cannot break the existing intramolecular hydrogen bond.

The fluorescence emission spectra measured in 15 solvents of varying polarity and are shown in Fig. S8A and S8B. In the fluorescence emission spectra resolved peaks were detected in 15 solvents. The fluorescence maximum shifts to red with increasing solvent polarity. Emission occurs at longer wavelength when compared with absorption. This indicates that the dipole moment of compounds **(1)** and **(2)** in the excited state (μ_e) is greater than the dipole moment of compounds **(1)** and **(2)** in the ground state (μ_g), which corresponds to an intramolecular charge transfer accompanying the excitation to the lowest excited singlet state. An increase in the solute dipole moment increases the intermolecular interaction between the solvents and the excited molecule. So, potential energy of the excited molecules decreases in polar solvents.

Estimation of the dipole moment ratio

Determination of the dipole moment ratio between excited and ground state of the compounds **(1)** and **(2)** are possible from the absorption and emission spectra measured in 15 solvents of different polarity. The slope m_1, between $f(\varepsilon_r, n)$ and $\upsilon_a - \upsilon_f (cm^{-1})$ and slope m_2 between $f(\varepsilon_r, n) + 2g(n)$ and $\upsilon_a + \upsilon_f (cm^{-1})$ are obtained from Fig. S9 and S10. The photophysical parameters are tabulated in Table S1. From the slope values m1 and m2, the ratio of excited state to ground state dipole moment of the solute was calculated using the following equation.

$$(\mu_e)/(\mu_g) = m1 + m2/m2 - m1$$

The ratio of dipole moment in the excited state and ground state of compound **(1)** and **(2)** are found to be $((\mu_e)/(\mu_g))$ 3.76 and 2.13 respectively.

pH titration of compounds (1), (2) and their pKa values

pH titrations were carried out for both the compounds between pH range 1-13 to study the change in absorbance behavior and also to calculate pKa values as shown in Fig. S11 for compounds **(1)** and **(2)**, it is evident that there is a considerable red shift observed over and above pH 7 without much change in the λ_{max} but absorption intensity increases up to pH 10, beyond that there is no appreciable change in the intensity. But in the acidic pH there is a considerable blue shift observed and the intensity decreases with increase in pH.

There pH titration results were used to calculate the pKa values of compounds **(1)** and **(2) as per** the methods available in the literature[37, 38]. Intensities and corrected intensities for λ_{acidic} and λ_{basic} for compounds (1) and (2) are listed in Table S3 and S4. These studies were carried out based on Hendersan-Hasselbach equation, as shown in Fig. S12 the pKa of Compounds (1), **(2) are** 7.4 and 7.0 respectively. The details are explained in the supplementary section.

Chemosensor

The fluorescence response of the sensors **(1)** and **(2)** to various cations and its selectivity for Zn^{2+} chemosensor are explained by the mechanism of electron transfer (ET) and intermolecular charge transfer (ICT). The fluorescence emission spectra of 10 μM solutions of the sensor **(1)** and **(2)** were investigated in ethanol-water (4: 1, v/v) solution.

We observed the changes in its photonic properties with the addition of metal ions like Cd^{2+}, Pb^{2+}, Ni^{2+}, Ag^+, Hg^{2+}, Cu^{2+}, Mn^{2+}, Fe^{2+}, Fe^{3+}, Al^{3+} Cr^{3+}, K^+, Na^+ and Co^{2+}. Upon the addition of Zn^{2+}, it induces fluorescence of **(1)** and **(2)** enormously (Fig. 3a and 4a). This large fluorescence enhancement with Zn^{2+} can be ascribed to the blocking of the ET process from nitrogen in the hydrazone moiety to dione, as shown in Fig.3a and 4a compounds **(1)** and **(2)** exhibited a selective fluorescence enhancement only with Zn^{2+} with maximum emission at 455 nm in **(1)** and 485 nm in **(2)** (Fig. 3a and 4a). In contrast, other metal ions did not induce significant fluorescence enhancement of **(1)** and **(2).** To understand the interactions between compound **(1)**, compound **(2)** and Zn^{2+}, the fluorescence variations of compounds **(1)** and **(2)** were measured upon the addition of various concentrations Zn^{2+}. The emission around 455 nm for (1) and 485 nm for (2) did not change when the concentration of Zn^{2+} is increased from 1 μmol/L compound **(1) and (2)** in 1:1(volume ratio) CH_3CH_2OH/H_2O (10 mmol/L 10 μM HEPES buffer, pH=7.0) binding to Zn^{2+} with different concentrations. It implies 1:1 complexation of compounds (**1**) and (**2**) with Zn^{2+} ions (Fig. 3B and 4B). The maximum fluorescence enhancement was observed in the presence of 3.5 μM **(1)** and 4.0 μM in **(2)**. When the concentration of Zn^{2+} was less or equal to around 3.5 μM (1) and 4.0 (2), the binding of Zn^{2+} made the polarization of the molecule larger, and it allowed only partial electron transfer and therefore the fluorescence intensity was enhanced, but the emission maximum does not change with the increase of Zn^{2+} concentration; At the same time, when the concentration of Zn^{2+} was above 3.5 μM or 4.0 μM, excess Zn^{2+} resulted in a sudden drop of relative intensity due to concentration quenching. Therefore, we limited the concentration to 10 μM and the limits of detection (LOD) were to 3.5 μM **(1)** and to 4.0 μM **(2)**.

Furthermore, it is well known in coordination chemistry that the complexation of Zinc with a ligand containing at least two nitrogen donor atoms is favored by the activation of the inert pair of the Zn^{2+} ion, leading to the shortening of the Zn–N bond length and much stronger covalent bonding. To further investigate the selectivity for Zn^{2+} ions, over other competitive metal ion binding studies shown in Fig. S16 clearly indicate the non-interference of the other metal ions (5 equivalents) on the Zn^{2+} selective detection by sensor **(1)** and **(2)**. These results suggested that compounds **(1)** and **(2)** can be used as potential chemosensors for the Zn^{2+} ion. The nitrogen lone pair of electrons is expected to contribute to the fluorophore, which can be tuned by metal coordination because fluorescence quenching occurs via electrons of the lone pair of nitrogen. This quenching is removed by complex formation with Zn^{2+} which enhances the fluorescence intensity

In addition, the spectroscopic responses were reversible. When the Zn^{2+} chelating reagent $EDTANa_2$ (1.0 equiv.) was added to **(1)** – Zn^{2+} and **(2)** – Zn^{2+} solutions (Fig. S13 and S14), the fluorescence spectra were almost restored to their original shapes for the free compound **(1)** and **(2)**, which indicates the effective removal of Zn^{2+}. This phenomenon proves that these compounds could serve as selective "turn–on" sensors for Zn^{2+}.

For the reuse of sensors we studied the emission spectrum of sensors (1) and (2) by further addition of Zn^{2+} as mentioned above which turned on fluorescence again. It was again quenched by adding an equivalent amount of EDTA. The procedure was repeated for 7 times. Up to 3 addition the fluorescence recovery was equivalent to the first addition and in the fourth and fifth additions there is decreasing in intensity as shown in the Fig.S13 and

S14 Further addition of Zn^{2+} does not change the spectrum due to concentration quenching and large amount of EDTA which is present

The influence of pH on the chemosensors **(1)** and **(2)** were studied using UV-Visible spectrometry (Fig. 5a and b). Over a pH range of 3–8, the visible absorption bands centered at 410 nm for sensor **(1)** and 430 nm for sensor **(2)** were unaltered. But an increase in pH from 9 to 11 engendered a shift in the maximum absorption wavelength to 350 nm (1) and 370 nm (2) without color change of yellow solution. This difference was due to the dissociation of the **(1)**– Zn^{2+} and **(2)**– Zn^{2+} complexes, which resulted in a lower absorbance value. The absorption intensities of **(1)** and **(2)** with Zn^{2+} increased dramatically from pH 3 to 8, resulting from the competition between the N–H proton and Zn^{2+} ion.[39, 40] In particular, significant changes in the absorbance spectra were observed in the range of pH 9–11, and the absorbance intensities decreased under alkaline conditions. The quenching at a higher pH could be well explained by the formation of $Zn(OH)_2$ and thus a reduction in the concentration of Zn^{2+}–1/2.[41] occurs from the above result, it shows that the effect of pH on compound 1/2– Zn^{2+} is the stable fluorescence intensity at a pH range from 3 to 8. So we have carried out **(1)** and **(2)** compounds in neutral limits. The absorption spectra of compounds **(1)** and **(2)** are generally bathochromatically shifted with respect to corresponding azo tautomers. The effect of polar substituent on absorption maxima is mutually opposite.[42, 43] Only hydrazone fluorescence was observed, where both tautomers were present, and thus excited state intramolecular proton transfer process (from oxygen to nitrogen) was detected by comparison of absorption and fluorescence excitation spectra.[44, 45] The manifest coordinating capability of the nitrogen could induce the formation of stable

complexes of the Zinc with potential photophysical properties. Many analytical techniques

based on sample destructive methods can be used to detect this metals.[46]

Molecular Docking Interaction of Compound (1) and (2) with 4–LRH

The compounds **(1)** and **(2)** are docked to the model of 4–LRH showing good fit and

favorable interactions that confirmed the assumed ligand binding mode at those targets. The

3-D images of hydrogen bond interaction and ribbon model docking of compound (1) and

(2) with 4-LRH protein are shown in Fig. 6a, b and 7a, b. Because 4–LRH was considered a

highly desirable feature of these ligands, in order to assess the possibility of its interactions

with this target or potential modifications required for this activity to occur. Compound **(1)**

is stabilized through specific interactions such as hydrogen bonding and nonspecific

interactions such as hydrophobic interactions with residues in the drug-binding pocket of

4LRH. The hydrogen bond acceptor oxygen atom at the ortho-position of the

dimethylcyclohexane-1,3-dione moiety showed hydrogen bonding interaction with the side

chain of HIE 135. It seems that the addition of a two carbonyl group and one nitrazo group

at position 2 and 1 of the dimethylcyclohexane-1,3-dione, which was demonstrated to form a

key H-bond with HIE 135, may be favorable to enhance the inhibitory activity against the

KB cell line. The cation (metal) interaction with the ASH 81, polar interaction with THR 82,

HIE 135, as well as the hydrophobic interactions with TYR 85, TRP 64, PHE 62, TRP 140,

TRP 134, TRP 138, TRP 102, TYR 60 and TRP 171. The modeling suggests that the phenyl

group of compound 1 form a parallel, $\pi - \pi$ stacked arrangement with TRP 140. Thus,

according to the chemical structures of these inhibitors, we speculate that the one aromatic

ring and one dimethylcyclohexane-1,3-dione, with dimethylcyclohexane-1,3-dione

possessing a carboxyl group, linked by a polar group may be an important structural feature of inhibitors (HIE 135) (Fig. 8).

Cytotoxicity

The cytotoxicity responses of **(1)** and **(2)** with various concentrations added are clearly evident from the cellular imaging. Hence, these results indicate that **(1)** and **(2)** are an efficient candidate for monitoring changes in the intracellular concentration under certain biological conditions; in order to test its cytotoxicity, we performed MTT assay in human KB cancer cells treated with various concentrations of compounds **(1)** and **(2)** for up to 5 h. As shown in Fig. 8 A1-A3 and B1-B3. 20 μM concentrations of compounds **(1)** and **(2)** show significant cytotoxic effects on KB cancer cells for at least up to 4 h. The synthesized compound **(1)** and **(2)** were examined for their cytotoxic properties on KB cell line by means of MTT test that allows us to evaluate the toxic effect of complexes on cellular mitochondrial metabolism. Cells were tested for 48 h with increasing concentrations of testing compounds. Cytotoxicity results are given in Table S2. Microscopic images of control cancer cells and apoptotic morphological changes in KB cell line treated with compound **(1)** and **(2)** are shown in Fig. 8. The results indicate that the compound **(1)** showed minimum cell death when compared to compound **2**. The compounds **1** and **2** exhibit broad inhibition on the KB cell lines with IC50 values of 50.60 and 60.80 respectively. The IC50 values of the compound (Fig. S15) suggest that compound **1** posses most potent inhibitory effect against the cancer cells. Compound **1** carrying the –NO$_2$ group in ortho position and shows the highest IC50 value, compelling us to propose that the electronic effect may be one of the factors in determining the anticancer activities of a compound **(2)**.[47, 48]

Molecular orbital studies

The HOMO–LUMO energies were also calculated and shown in Fig. 10. The highest occupied molecular orbital (HOMO) and the lowest unoccupied molecular orbital (LUMO) are the main orbitals that take part in chemical stability.[49] The HOMO represents the ability to donate an electron, LUMO as an electron acceptor represents the ability to loss obtain an electron. The value of energy separation between the HOMO and LUMO are 4.4211 (1) and 3.3200 (2) respectively. The chemical hardness and softness of a molecule is a good indication of the chemical stability of a molecule. From the HOMO–LUMO energy gap, one can find whether the molecule is hard or soft. The molecules having a large energy gap are known as hard, and molecules having small energy gap is known as soft molecules. The soft molecules are more polarizable than the hard ones, because they need small energy for excitation. The hardness value of a molecule can be determined by the formula.[50]

$$\eta = \frac{\varepsilon_{HOMO} + \varepsilon_{LUMO}}{2}$$

Where ε_{HOMO} and ε_{LUMO} are the energies of the HOMO and LUMO molecular orbitals. The value of η (Hardness) of the **(1)** and **(2)** molecules are 2.2105 eV and 1.6600 eV. Hence, from the calculation; we conclude that the molecules were taken under investigation belongs to the hard materials.

Molecular electrostatic potential (MEP) maps

To predict reactive sites for electrophilic and nucleophilic attack for the investigated molecule, MEP is calculated (red is negative, blue is positive) at the B3LYP/6−31G

optimized geometries. Fig. 11 shows the calculated 3D electrostatic potential contour map of **1** and **2**. The different values of the electrostatic potential at the surface are represented by different colors. Electrostatic potential increases in the order red < orange < yellow < green < blue. The color code of these maps is in the range between$-6.363e^{-2}$ (deep red) to $6.363e^{-2}$ (deep blue) in compound **1** and $-6.478e^{-2}$ (deepest red) to $6.478\ e^{-2}$ (deep blue) in compound 2, where blue indicates the strongest attraction and red indicates the strongest repulsion. From this result, it is clear that the H atoms indicate the strongest attraction and O atoms indicate the strongest repulsion.

Charge distribution

The charge distribution of the molecule was calculated on the basis of Mulliken method using a B3LYP/6-31G level calculation. This calculation depicts the charges of the every atom in the molecule. Distributions of positive and negative charges are the vital to increase or decrease of bond length between the atoms. Mulliken atomic charges and the plot have shown in Fig. S17. The bar diagram clearly shows the donor atom of negative charges and the acceptor atom of positive charges.

Conclusion

In summary, the compound **(1)** and **(2)** have been synthesized and characterized by IR, ^{1}H, ^{13}C NMR spectra studies. When a Zinc ion was added in **(1)** and **(2)** their morphological changes were observed by SEM analysis. We have prepared a simple type of fluorescent "Turn–on-off" chemosensor based on hydrazones which shows interesting properties such as high sensitivity for Zn^{2+}. It possesses a high affinity and selectivity for Zinc ions relative to most other competitive metal ions by enhancement of the monomer fluorescence emission

of hydrazones in organic aqueous solution. We expect that the present design strategy and the remarkable photophysical properties of this sensor will help to extend the applications of fluorescent sensors for metal ions. In this present investigation, molecular structure, HOMO, LUMO, NBO, Mulliken charges and MEP analysis have been studied using ab initio DFT B3LYP/6-31G calculation.

References and notes

1 O. T. Butler, J. M. Cook, C. F. Harrington, S. J. Hill, J. Rieuwerts and D. L. Miles, *J. Anal. At. Spectrom.*, 2006, **21**, 217.

2 A. W. Czarnik, Fluorescent Chemosensors for Ion and Molecule Recognition; ACS: Washington, DC, 1992.

3 J. R. Lakowicz, Principles of Fluorescence Spectroscopy; Plenum Press: New York, 1983.

4 J. R. Lakowicz, Fluorescence spectroscopy of biomolecules. In Encyclopedia of molecular biology and molecular medicine; Meyers, R. A., Ed.; VCH Publishers: New York, 1995.

5 H. Szmacinski, I. Gryczynski and R. Lakowicz, *J. Photochem. Photobiol.*, 1993, **58**, 341.

6 T. Yanagida and Y. Ishii, Single Molecule Dynamics in Life Science; Wiley-VCH: Weinheim, Germany, 2009.

7 T. Dudev, *Chem. Rev.,* 2003, **103**, 773.

8 J. H. Laity, B. M. Lee and P. E. Wright, *Curr. Opin. Struct. Biol.,* 2001, **11**, 39.

9 J. M. Berg, Y. G. Shi, *Science* 1996, **271**, 1081.

10 B. K. Datta, S. Mukherjee, C. Kar, A. Ramesh, and G. Das, *Anal. Chem.,* 2013, **85**, 8369.

11 B. L. Vallee and K. H. Falchuk, *Physiol. Rev.,* 1993, **73**, 79.

12 (a) A. I. Bush, *Curr. Opin. Chem. Biol.,* 2000, **4**, 184; (b) C. J. Frederickson, S. C. Burdette, C. J. Frederickson, S. L. Sensi, J. H. Weiss, H. Z. Yin, R. V. Balaji, A. Q. Truong-Tran, E. Bedell, D. S. Prough and S. J. Lippard, *J. Neurosci. Methods,* 2004, **139**, 79.

13 A. Scrimgeoura, C. H. Stahl, J. P. McClung, L. J. Marchitelli and A. J. Young, *J. Nutr. Biol.,* 2007, **18**, 813.

14 A. P. de Silva, H. Q. Nimal Gunaratne, T. Gunnlaugsson, A. J. M. Huxley, C. P. McCoy, J. T. Rademacher and T. E. Rice, *Chem.Rev.,* 1997, **97**, 1515.

15 C. J. Frederickson, J. Y. Koh and A. I. Bush, *Nat. Rev. Neurosci.,* 2005, **6**, 449.

16 A. I. Bush, W. H. Pettingell, G. Multhaup, M. Paradis, J. P. Vonsattel, J. F. Gusella, K. Beyreuther, C. L. Masters and R. E. Tanzi, *Science,* 1994, **265**, 1464.

17 Z. Xu, J. Yoon and D. Spring, *Chem. Soc. Rev.,* 2010, **39**, 1996.

18 L. Zhu, Z. Yuan, J. T Simmons and K. Sreenath, *RSC Adv.,* 2014, **4**, 20398.

19 E. L. Que, D. W. Domaille and C. J. Chang, *Chem. Rev.,* 2008, **108**, 1517.

20 P. Jiang and J. Guo, *Coord. Chem. Rev.,* 2004, **248**, 205.

21 P. Carol, S. Sreejith and A. Ajayaghosh, *Chem. Asian J.,* 2007, **2**, 338.

22 E. Kimura and S. Aoki, *BioMetals,* 2001, **14**, 191.

23 R. J. Radford, W. Chyan and S. J. Lippard, *Chem. Sci.*, 2013, **4**, 3080-3084.

24 Y. Mikata, Y. Nodomi, A. Kizu and H. Konno, *Dalton Trans.,* 2014, **43**, 1684.

25 J. T Simmons, Z. Yuan, K. L Daykin, B. T Nguyen, R. J Clark, M. Shatruk and L. Zhu, *Supramol. Chem.,* 2014, **26**, 214.

26. K. Sreenath, Z. Yuan, J. R Allen, M. W Davidson and L Zhu, *Chem. Eur. J.,* 2014, **20**, 1–9.

27 F. R. Pavan, P. I. D. S. Maia, S. R. A. Leite, V. M. Deflon, A. A. Batista, D. N. Sato, S. G. Franzblau and C. Q. F. Leite, *Eur. J. Med. Chem.,* 2010**, 45***,* 1898.

28 W. Retting, B. Strehmel, B. Schroder and H. Seifert, ed., Applied Fluorescence in Chemistry, Biology and Medicine, Springer-Verlag, New York, **1999**.

29 J. R. Lakowicz, Principles of Fluorescence Spectroscopy, Springer Science + Business Media, New York, **2006**.

30 Z. Xu, J. Yoon and D. R. Spring, *Chem. Soc. Rev.,* 2010, **39***,* 1996.

31 K. Kikuchi, *Chem. Soc. Rev.,* 2010, **39***,* 2048.

32 J. Wu, W. Liu, J. Ge, H. Zhang and P. Wang, *Chem. Soc. Rev.*, 2011, **40***,* 3483.

33 D. T. Quang and J. S. Kim, *Chem. Rev.,* 2010, **110***,* 6280.

34 S. Denizot and R. Lang, *J. Immunol. Methods* 1986*,* **89**, 271.

35 Gaussian 03 Program, Gaussian Inc., Walling ford CT, 2004.

36 H. B. Schlegel, *J. Comput. Chem.,* 1982, **3** 214.

37 R. D. Barun, Introduction to chemical Analysis; McGraw-Hill, New York, 1982, pp. 197-199.

38 G. H. Jeffery, H. Bassett, J. Mendam and R.C. Denny, "Vogel's Text books of quantitative chemical Analysis, 5 edn., 1989, pp. 46-49.

39 L. Xue, G. P. Li, D. J. Zhu, Q. Liu and H. Jiang, *Inorg. Chem*., 2012, **51**, 10842.

40 Y. Zhang, X. F. Guo, W. X. Si, L. H. Jia and X. H. Qian, *Org. Lett*., 2008, **10**, 473.

41 X. Y. Zhou, B. R. Yu, Y. L. Guo, X. L. Tang, H. H. Zhang and W. S. Liu, *Inorg. Chem.,* 2010, **49**, 4002.

42 K. T. Mahmudova, M. N. Kopylovich and A. J. L. Pombeiro, *Coord. Chem. Rev.,* 2013, **257**, 1244; (b) A. Sethukumar and B. A. Prakasam, *J. Mol. Struct.*, 2010, **963,** 250.

43 J. Griffiths, *J. Soc. Dyers Colour.,* 1972;**88**, 106.

44 M. H. R. Bartel, *J. Prakt. Chem.,* 1982, **324**, 743.

45 P. Nikolov, F. Fratev, S. Stoyanov and O. E. Polansky, *Z. Naturforsch., B: Chem. Sci.,* 1981, **36,** 191.

46 H. Joshi, F. S. Kamounah, C. Gooijer, G .V. D. Zwan and L. Antonov*, J. Photochem. Photobiol., A* 2002, **152**, 183.

47 V. G. Sankareswari, D. Vinod, A. Mahalakshmi, M. Alamelu, G. Kumaresan, R. Ramaraj and S. Rajagopal, *Dalton Trans.,* 2014, **43,** 3260.

48 Y. Zhang, X. Wang, W. Fang, X. Cai, F. Chu, X. Liao and J. Lu, *J. Bioinorg. Chem. Appl.,* 2013, 1.

49 S.Gunasekaran, R.A. Balaji, S. Kumaresan, G. Anand, S. Srinivasan, *Can. J. Anal. Sci. Spectros.* 2008, **53,**149.

50 K. Fukui, *Science,* 1982, **218**, 747.

Graphical Abstract
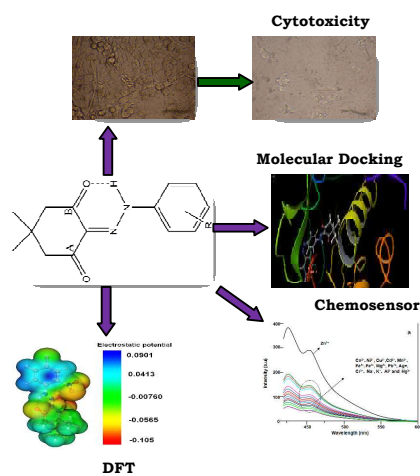
Arylhydrazone based new Zn^{2+} "ON–OFF" chemosensors in neutral aqueous ethanol medium have been designed by simple method. Additionally their cytotoxic activity towards KB cell and molecular docking with 4LRH cancer proteins also investigated.

Figure captions and Scheme

Fig.1 SEM image of compound (1) at (a) 10 μm (c) 5 μm and its Zn^{2+} complex at (b) 10 μm (d) 5 μm.

Fig. 2 SEM image of compound (2) at (a) 20 μm (c) 10 μm and its Zn^{2+} complex at (b) 10 μm (d) 10 μm.

Fig. 3 (A) Fluorescence emission spectra of 10 μM solutions of the chemosensor **(1)** with different metal ions (perchlorate, chloride, or nitrate salts of Zn^{2+}, Co^{2+}, Ni^{2+}, Cu^{2+}, Pb^{2+}, Hg^{2+}, Mg^{2+}, Cr^{3+}, Na^+, K^+, Fe^{2+}, Fe^{3+}, Al^{3+}, Cd^{2+} , Mn^{2+} and Ag^+ in aq. CH_3CH_2OH ($CH_3CH_2OH–H_2O$ 4/1, v/v, 10 μM HEPES buffer, pH 7.0). **(B)** Emission spectra of compound (1) in the presence of an increasing Zn^{2+} concentration Zn^{2+} /(μmol L^{-1}) from **(a to n)** 0, 0.2, 0.6, 0.8, 1.2, 1.5, 1.9, 2, 2.3, 2.6, 3.0, 3.5, 4.0, 4.5 1 μmol/L compound **(1)** in 1:1(volume ratio) CH_3CH_2OH/H_2O (10 mmol/L 10 μM HEPES buffer, pH=7.0) binding to Zn^{2+} with different concentrations.

Fig. 4 (A) Fluorescence emission spectra of 10 μM solutions of the chemosensor **(2)** with different metal ions (perchlorate, chloride, or nitrate salts of Zn^{2+}, Co^{2+}, Ni^{2+}, Cu^{2+}, Pb^{2+}, Hg^{2+}, Mg^{2+}, Cr^{3+}, Na^+, K^+, Fe^{2+}, Fe^{3+}, Al^{3+}, Cd^{2+}, Mn^{2+} and Ag^+ in aq. CH_3CH_2OH ($CH_3CH_2OH–H_2O$ 4/1, v/v, 10 μM HEPES buffer, pH 7.0). **(B)** Emission spectra of compound (2) in the presence of an increasing Zn^{2+} concentration Zn^{2+} /(μmol /L) from **(a to o)** 0, 0.2, 0.6, 0.8, 1.2, 1.5, 1.9, 2, 2.3, 2.6, 3.0, 3.5, 4.0, 4.5, 5.0 1 μmol/L compound **(1)** in 1:1(volume ratio) CH_3CH_2OH/H_2O (10 mmol/L 10 μM HEPES buffer, pH=7.0) binding to Zn^{2+} with different concentrations.

Fig. 5 Absorbance spectra of (A) and (B), compound **(1)** and compound **(2)** in ethanol: H_2O with Zn^{2+} Solution at different pH. (a-i) pH = 3 to pH = 11 respectively.

Fig. 6 Molecular docking studies of compound **(1)** with 4LRH.

Fig. 7 Molecular docking studies of compound **(2)** with 4LRH.

Fig. 8 2–D images of Molecular docking studies of compound **(1)** and **(2)** with 4LRH Protein residues.

Fig. 9 Live Cell images of compound **(1)**: (left) (A1) before and (A2 and A3) after treatment with Compound **(1)** examined by fluorescence microscopy (right). Live Cell images of compound **(2)**: (B1) before and (B2 and B3) after treatment with Compound (2) examined by fluorescence microscopy.

Fig. 10 HOMO-LUMO energy gap of compound **(1)** and compound **(2).**

Fig. 11 MEP diagrams. (A) compound **(1)** and (B) compound **(2).**

Fig. 12 Intramolecular charge transfer structure of compound **(1)** and **(2).**
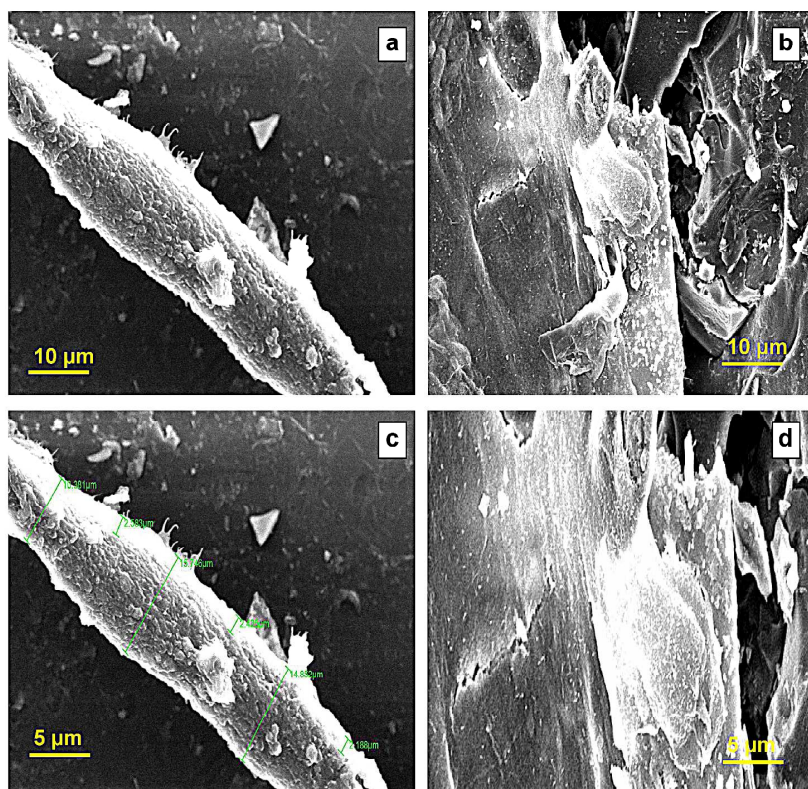
Fig. 1
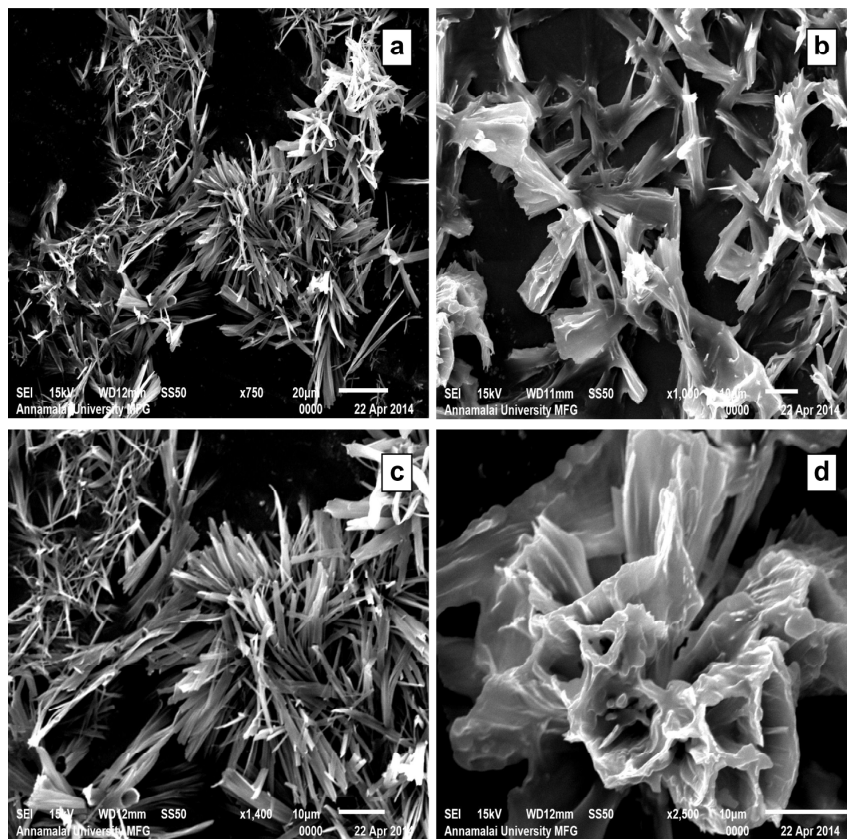
Fig. 2
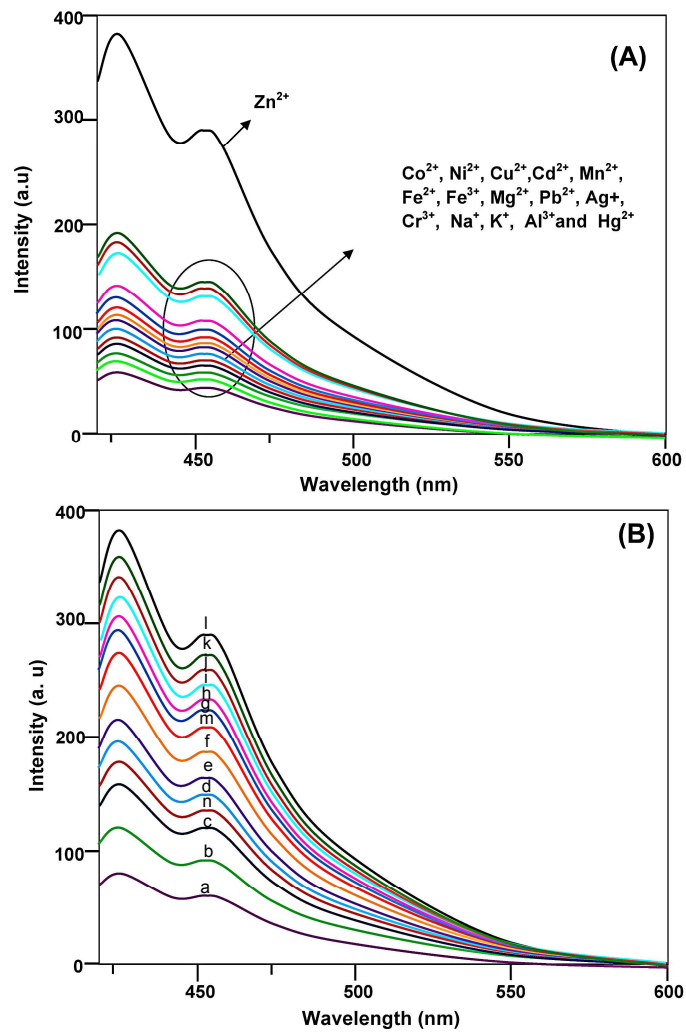
Fig. 3

Fig. 4

Fig. 5

Fig. 6

Fig. 7

Fig. 8

Fig. 9

HOMO = − 4.8402 eV

ΔE = 0.5217 eV

LUMO = − 4.318 eV

Compound 1

HOMO = − 1.925 eV

ΔE = 1.4944 eV

LUMO = − 3.4202 eV

Compound 2

Fig. 10

(A)

Electrostatic potential

0.0901

0.0413

-0.00760

-0.0565

-0.105

(B)

Electrostatic potential

0.0398

0.00858

-0.0227

-0.0539

-0.0852
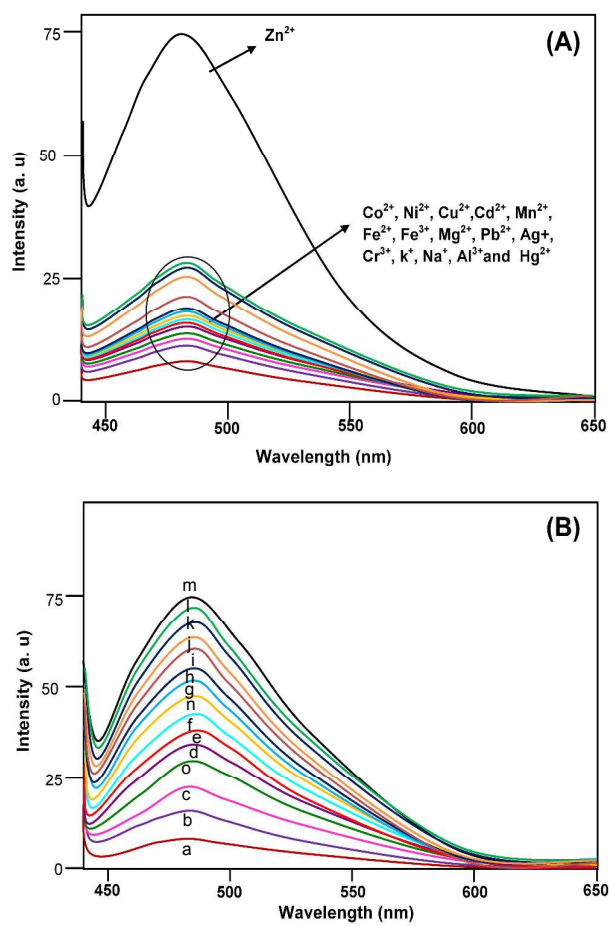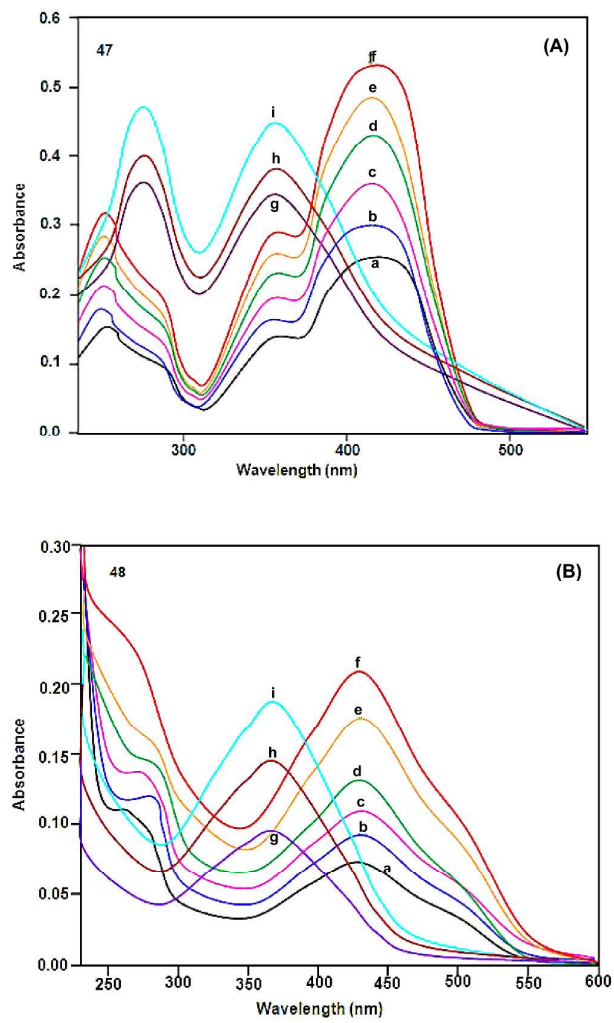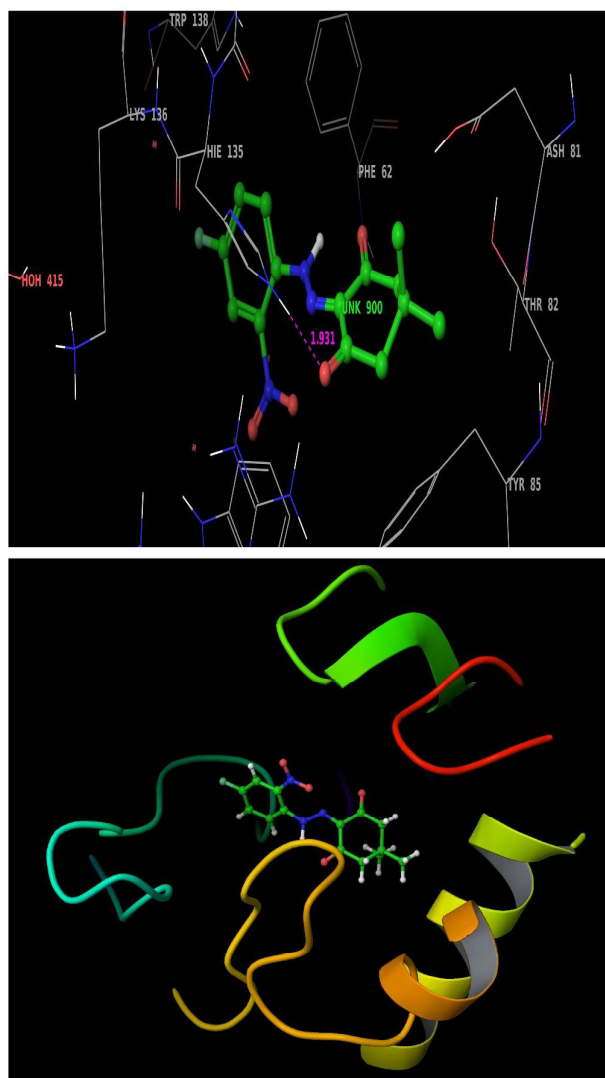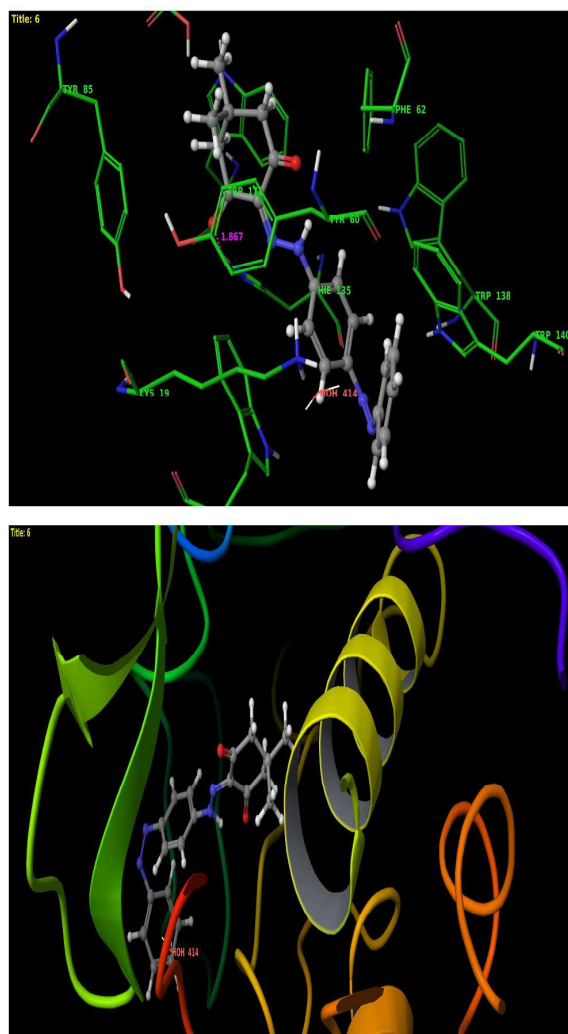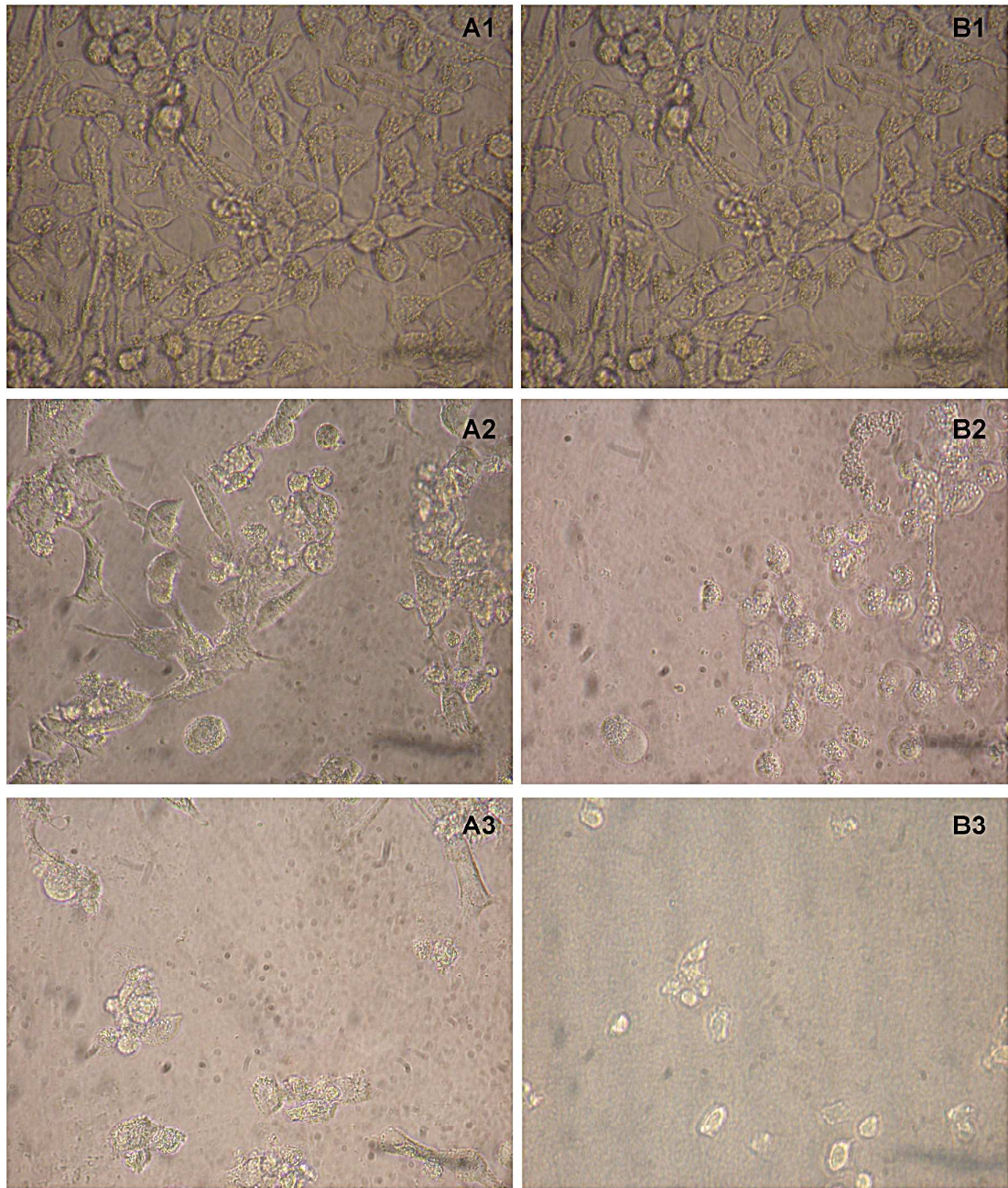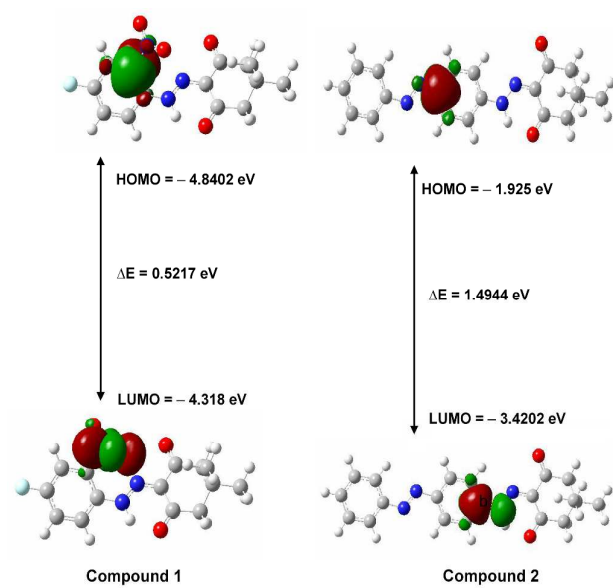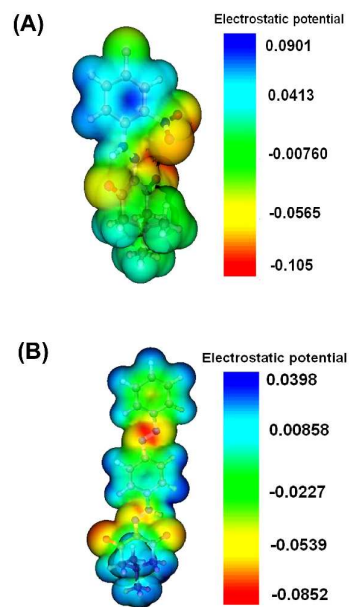
Fig. 11

R = Compound **(1) 4-F, 2-NO₂,**

Compound **(2) phenyldiazenyl**

Fig. 12

R = Compound **(1) 4-F, 2-NO₂,**

Compound **(2) phenyldiazenyl**

Compounds **(1) and (2)**
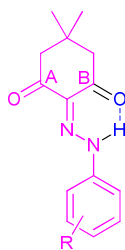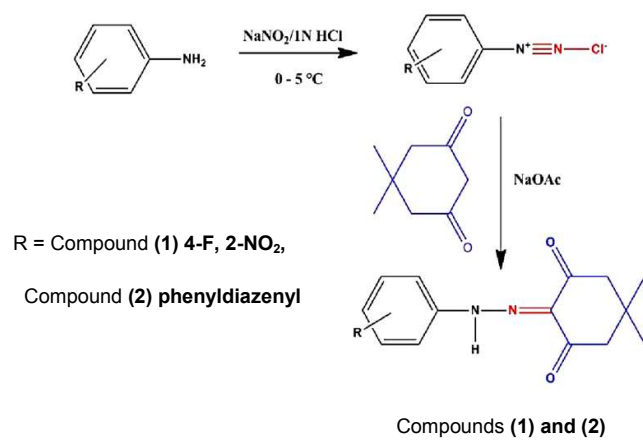
Sheme 1. Schematic representation of synthesis of aryl Hydrozone.